



University of Kentucky
UKnowledge

Physics and Astronomy Faculty Publications

Physics and Astronomy

2007

Discovery of Atomic and Molecular Mid-Infrared Emission Lines in Off-Nuclear Regions of NGC 1275 and NGC 4696 with the *Spitzer Space Telescope*

R. M. Johnstone
University of Cambridge, UK

N. A. Hatch
University of Cambridge, UK

Gary J. Ferland
University of Kentucky, gary@uky.edu

A. C. Fabian
University of Cambridge, UK

C. S. Crawford
University of Cambridge, UK

See next page for additional authors

Follow this and additional works at: https://uknowledge.uky.edu/physastron_facpub

 [Click here to open a feedback form in a new tab to let us know how this document benefits you.](#)

Part of the [Astrophysics and Astronomy Commons](#), and the [Physics Commons](#)

Repository Citation

Johnstone, R. M.; Hatch, N. A.; Ferland, Gary J.; Fabian, A. C.; Crawford, C. S.; and Wilman, R. J., "Discovery of Atomic and Molecular Mid-Infrared Emission Lines in Off-Nuclear Regions of NGC 1275 and NGC 4696 with the *Spitzer Space Telescope*" (2007). *Physics and Astronomy Faculty Publications*. 43.
https://uknowledge.uky.edu/physastron_facpub/43

This Article is brought to you for free and open access by the Physics and Astronomy at UKnowledge. It has been accepted for inclusion in Physics and Astronomy Faculty Publications by an authorized administrator of UKnowledge. For more information, please contact UKnowledge@lsv.uky.edu.

Authors

R. M. Johnstone, N. A. Hatch, Gary J. Ferland, A. C. Fabian, C. S. Crawford, and R. J. Wilman

Discovery of Atomic and Molecular Mid-Infrared Emission Lines in Off-Nuclear Regions of NGC 1275 and NGC 4696 with the *Spitzer Space Telescope***Notes/Citation Information**

Published in *Monthly Notices of the Royal Astronomical Society*, v. 382, issue 3, p. 1246-1260.

This article has been accepted for publication in *Monthly Notices of the Royal Astronomical Society* ©: 2007 The Authors Published by Oxford University Press on behalf of the Royal Astronomical Society. All rights reserved.

The copyright holder has granted the permission for posting the article here.

Digital Object Identifier (DOI)

<https://doi.org/10.1111/j.1365-2966.2007.12460.x>

Discovery of atomic and molecular mid-infrared emission lines in off-nuclear regions of NGC 1275 and NGC 4696 with the *Spitzer Space Telescope*

R. M. Johnstone,^{1★} N. A. Hatch,^{1,2} G. J. Ferland,³ A. C. Fabian,¹ C. S. Crawford¹
and R. J. Wilman^{4,5}

¹*Institute of Astronomy, University of Cambridge, Madingley Road, Cambridge CB3 0HA*

²*Leiden Observatory, P.B. 9513, Leiden 2300 RA, the Netherlands*

³*Department of Physics, University of Kentucky, Lexington, KY 40506, USA*

⁴*Department of Physics, University of Durham, South Road, Durham DH1 3LE*

⁵*Astrophysics, University of Oxford, Denys Wilkinson Building, Oxford OX1 3RH*

Accepted 2007 September 11. Received 2007 September 4; in original form 2007 February 16

ABSTRACT

We present *Spitzer* high-resolution spectra of off-nuclear regions in the central cluster galaxies NGC 1275 and NGC 4696 in the Perseus and Centaurus clusters, respectively. Both objects are surrounded by extensive optical emission-line filamentary nebulae, bright outer parts of which are the targets of our observations. The 10–37 μm spectra show strong pure-rotational lines from molecular hydrogen revealing a molecular component to the filaments which has an excitation temperature of ~ 300 – 400 K. The flux in the 0–0 S(1) molecular hydrogen line correlates well with the strength of the optical lines, having about 3 per cent of the $\text{H}\alpha + [\text{N II}]$ emission. The 11.3- μm polycyclic aromatic hydrocarbon feature is seen in some spectra. Emission is also seen from both low- and high-ionization fine-structure lines. Molecular hydrogen cooler than ~ 400 K dominates the mass of the outer filaments; the nebulae are predominantly molecular.

Key words: galaxies: clusters: general – galaxies: clusters: individual: NGC 1275 – galaxies: clusters: individual: NGC 4696 – intergalactic medium – infrared: galaxies.

1 INTRODUCTION

The massive central galaxy in many clusters is often surrounded by an extensive emission-line nebulosity (e.g. Cowie et al. 1983; Johnstone, Fabian & Nulsen 1987; Heckman et al. 1989; Crawford et al. 1999). Such emission-line galaxies are always at the centre of highly peaked X-ray emission from an intracluster medium where the radiative cooling time of the intracluster gas at the centre is less than 1 Gyr (Fabian 1994; Peres et al. 1998; Bauer et al. 2005). Initially, the nebulosity was studied in the optical spectral region but strong ultraviolet (UV) and infrared (IR) lines have since been seen, together with dust which is inferred from the depletion of calcium, Balmer line ratios and dust lanes which are present in some cases. Recently, strong H_2 lines have been found (e.g. Jaffe & Bremer 1997; Edge et al. 2002, and references therein) as well as emission lines from the CO molecule (e.g. Edge 2001; Salomé & Combes 2003; Salomé et al. 2006).

The ionization, excitation, origin and fate of the filaments have been a long-standing puzzle. Most obvious sources of ionization, such as an active nucleus, a radio source, shocks, young stars and

conduction from the surrounding hot gas have drawbacks in one system or another.

XMM/Reflection Grating Spectrograph and *Chandra* X-ray spectra show that the intracluster gas in many cluster cores has a range of temperatures decreasing to about a factor of 3 below that of the outer hot gas, with very little X-ray emitting gas cooler than this (Peterson et al. 2001), indicating that some form of heating (e.g. from the central radio source, Churazov et al. 2002; Fabian et al. 2003a) is important and that it mostly balances the radiative cooling. Heating is unlikely to completely balance cooling over such an extended region, and so some residual cooling flow is expected to occur. Optically emitting warm gas filaments may be being dragged out from the central cluster galaxy by buoyant bubbles (Hatch et al. 2006) or may be a phase through which some gas passes in cooling out from the intracluster medium. The wider relevance of this issue is in the upper mass limit to the total stellar component of massive galaxies, which may be controlled by whatever heats cooling flows (Fabian et al. 2002b). If radiative cooling is not balanced in some way (or the cooled gas does not form stars) then the stellar component of cD galaxies should be much more massive than is observed, merely by the accretion of cooled intracluster gas. By measuring the quantity of young stars and warm/cold gas in these objects, we can determine how well heating balances cooling.

★E-mail: rmj@ast.cam.ac.uk

The emission-line filaments are markers of feedback in massive galaxies and to use them as such we need to understand their composition, origin and lifetime. Here, we study two of the brightest and most extensive emission-line nebulae around central cluster galaxies NGC 1275 (at redshift $z = 0.0176$, in the Perseus Cluster) and NGC 4696 (at redshift $z = 0.009867$, in the Centaurus cluster) using the *Spitzer* Infrared Spectrograph (IRS). The $H\alpha$ filaments around NGC 1275, which extend well beyond the body of the galaxy, have warm (2000 K) molecular hydrogen associated with them. This motivates us to search for much cooler (few times 100 K) molecular hydrogen in these regions using the rotational emission lines accessible to the IRS.

The central cD galaxy in the nearby Perseus cluster, NGC 1275, is surrounded by spectacular $H\alpha$ filaments which stretch over 100 kpc. These were first reported by Minkowski (1957) and imaged by Lynds (1970), McNamara, O’Connell & Sarazin (1996) and recently by Conselice, Gallagher & Wyse (2001). The Perseus cluster is the brightest cluster of galaxies (in flux units) at X-ray wavelengths with the emission peaking on NGC 1275 (Fabian et al. 1981, 2000, 2003a). The nucleus of NGC 1275 also powers an Fanaroff–Riley Class I radio source, 3C 84 (Pedlar et al. 1990). Bubbles of relativistic plasma have been blown by the jets from the nucleus and have displaced the X-ray emitting intracluster gas (Böhringer et al. 1993; Fabian et al. 2000; Churazov et al. 2001; Fabian et al. 2002a, 2003a). It is likely that the $H\alpha$ filaments avoid the bubbles in three-dimensional space, although there is no obvious anticorrelation as seen in projection on the sky; They appear to act like streamlines showing that the flow behind the outer bubble, and thus the whole inner medium, is not turbulent and may well have been dragged out from the central region (Fabian et al. 2003b; Hatch et al. 2006). Molecular hydrogen (Krabbe et al. 2000; Jaffe, Bremer & van der Werf 2001; Edge et al. 2002) and CO (Salomé et al. 2006, and references therein) have been observed and mapped in the inner regions for some time.

NGC 4696 at the centre of the Centaurus cluster has $H\alpha$ filaments discovered by Fabian et al. (1982) and a strong dust lane (Shobbrook 1966). Sparks, Macchetto & Golombek (1989) and Crawford et al. (2005) have mapped the nebulosity which appears to surround the dust lane.

The ionization state of the $H\alpha$ filaments in central cluster galaxies is low, with $[O\text{I}]\lambda 6300$, $[O\text{II}]\lambda 3727$ and $[N\text{II}]\lambda 6584$ being prominent in optical spectra as well as Balmer lines. Molecular H_2 is also common (e.g. Jaffe & Bremer 1997; Donahue et al. 2000; Edge et al. 2002), even in the outer filaments (Hatch et al. 2005). Egami et al. (2006) have recently found very strong rotational H_2 lines from the brightest cluster galaxy in Zw 3146, using *Spitzer* IRS data. Unlike with our objects, the emission is not spatially resolved due to the high redshift of the object ($z = 0.29$). The authors remark that this source has the most luminous pure-rotational H_2 lines and the largest mass of molecular hydrogen known in a brightest cluster galaxy. A *Spitzer* IRS spectrum of the centre of NGC 1275 is presented by Weedman et al. (2005). Forbidden atomic lines and at least one molecular line are seen sitting on a large continuum associated with the active nucleus. Kaneda, Onaka & Sakon (2005) and Kaneda et al. (2007) have taken low-resolution *Spitzer* IRS spectra of NGC 4696 and find polycyclic aromatic hydrocarbon (PAH) features and $[\text{Ne}\text{II}]$ line emission.

What is ionizing and exciting the filamentary gas remains uncertain. It is not simply an active nucleus (Johnstone & Fabian 1988; Sabra, Shields & Filippenko 2000), nor do a range of alternative mechanisms provide a comprehensive explanation (e.g. Crawford & Fabian 1992; Donahue et al. 2000; Sabra et al. 2000; Wilman et al.

2002). The UV emission from massive young stars is likely to play an important role (Johnstone et al. 1987; Allen 1995; Crawford et al. 1999), although this may not be the case for the outer filaments. The lifetime of the filaments is not known, although the immense size of the system around NGC 1275 (80 kpc) and the low-velocity spread seen in the filaments ($\sim 300\text{ km s}^{-1}$ or less) indicates that they may last over 10^8 yr.

In this paper, we present mid-IR *Spitzer* spectra of off-nuclear extended emission-line regions in NGC 1275 and NGC 4696. They probe a new region in temperature space ($\sim 300\text{--}400\text{ K}$) which lies between the very cold regions observed in transitions of the CO molecule and the warmer regions seen through ro-vibrational transitions of the hydrogen molecule. These emission-line filaments seem to be a key marker of feedback in cooling core clusters (Hu, Cowie & Wang 1985; Crawford et al. 1999) even though they do not contain a significant fraction of the total gas mass. It is by studying regions located away from the nucleus of the galaxies that we expect to be able to make progress in the understanding of the heating and ionization mechanisms of these filaments as they offer a simpler environment than is found close to the nuclei of the galaxies.

2 OBSERVATIONS AND DATA REDUCTION

2.1 Mid-IR *Spitzer* data

Spitzer IRS observations of off-nuclear regions in NGC 1275 and NGC 4696 were made during two observing campaigns in 2005 July and 2006 March (IRSX005200 and IRSX006300). For each object both the Short-Wavelength High-Resolution (SH) and Long-Wavelength High-Resolution (LH) spectrographs were used, giving an effective resolving power of $R \sim 600$ and a spectral coverage from ~ 10 to $\sim 37\ \mu\text{m}$. The entrance aperture size of the two spectrographs is rather different, being 4.7×11.3 arcsec for the SH and 11.1×22.3 arcsec for the LH spectrographs, respectively.

Table 1 lists details of the *Spitzer* observations. Three off-nuclear regions were observed in NGC 1275, chosen to be coincident with particular regions identified in the $H\alpha + [\text{N}\text{II}]$ map of Conselice et al. (2001), as well as a blank sky region. In NGC 4696, we covered the brightest part of the $H\alpha$ nebula to the south-west of the nucleus.

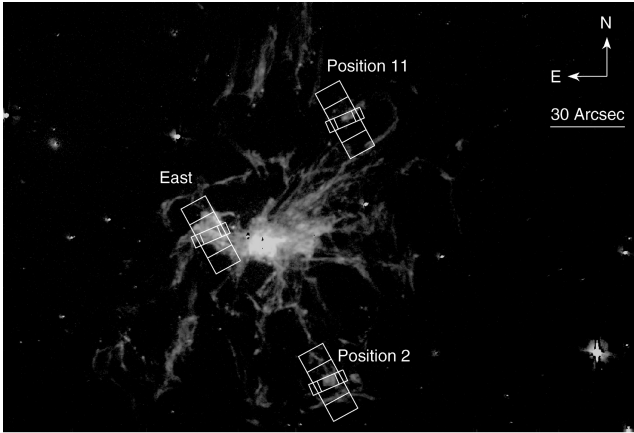
Figs 1 and 2 show the outline of the *Spitzer* spectrograph apertures overlaid on $H\alpha + [\text{N}\text{II}]$ images of the central cluster galaxies. There are two slightly different pointings (exposure ids) for each target position, these being the standard nod positions in the Staring Mode Astronomical Observation Template. These positions locate the target at one-third and two-thirds of the way along the spectrograph aperture. The SH spectrograph aperture positions are shown by the smaller rectangles whereas the LH spectrograph apertures are the larger rectangles which are approximately orthogonal to the SH spectrograph apertures. The specific pointing positions for each exposure id are given in Table 1.

The observations were processed by the *Spitzer* Science Centre through pipeline version S13.2.0. We use the ‘bcd.fits’, ‘func.fits’ and ‘bmask.fits’ files as the starting point for our reduction.

Individual Data Collection Event (DCE) files within each exposure id were first averaged together and an array of external uncertainties corresponding to the standard error on the mean was calculated. A new bmask file was also generated, this being the logical ‘or’ of all the bmask files for the input DCEs. The NGC 1275 east pointing has only one DCE in each spectrograph so in these cases the pipeline based uncertainties, which are computed from the ramp

Table 1. Log of *Spitzer* Observations.

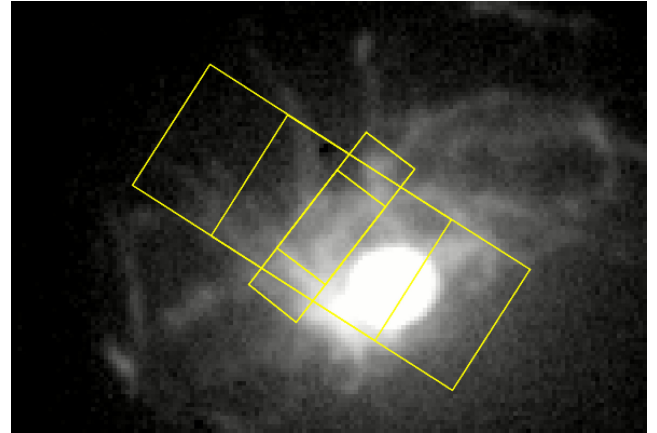
Target	Redshift	Observation date	Astronomical Observation	Request key	Mode	Exposure id	RA	Dec.	Exposure time	
							(2000)		(s)	
NGC 1275 east	0.0176	2006 March 14	r14536704		SH	0002	03:19:49.9	+41:30:48	481.69	
						0003	03:19:50.2	+41:30:46	481.69	
						LH	0004	03:19:49.9	+41:30:44	241.83
							0005	03:19:50.2	+41:30:50	241.83
							0002	03:19:45.7	+41:29:49	1445.07
NGC 1275 position 2	0.0176	2006 March 14	r14536448		SH	0003	03:19:46.0	+41:29:47	1445.07	
						LH	0004	03:19:45.7	+41:29:45	725.48
							0005	03:19:46.0	+41:29:51	725.48
							0002	03:19:45.0	+41:31:34	1445.07
						NGC 1275 position 11	0.0176	2006 March 14	r14536192	
LH	0004	03:19:45.0	+41:31:30	725.48						
	0005	03:19:45.3	+41:31:36	725.48						
	0000	03:19:53.6	+41:28:35	963.38						
NGC 1275 Blank	0.0176	2006 March 14	r16754176		SH					
						LH	0002	03:19:53.6	+41:28:31	483.65
							0003	03:19:53.9	+41:28:37	483.65
							0002	12:48:48.7	-41:18:42	2408.44
						NGC 4696	0.009 867	2005 July 9	r14537216	
LH	0004	12:48:48.5	-41:18:45	725.48						
	0005	12:48:49.1	-41:18:42	725.48						

**Figure 1.** *Spitzer* spectrograph apertures overlaid on an $H\alpha + [N II]$ image of the central region of NGC 1275 (Conselice et al. 2001). Small boxes show the positions of the SH spectrograph aperture while the larger boxes show the positions of the LH spectrograph aperture.

fitting of the multiple detector readouts, are used for the uncertainty arrays.

The NGC 1275 pointings were then background subtracted using the NGC 1275 blank field pointing, propagating the uncertainty arrays in quadrature and again creating a new bmask file that is the logical ‘or’ of the input masks.

In the case of the NGC 4696 pointing, we do not have a concurrent sky-background observation. For the LH data, we used an average of background observations (scaled to the expected background level at the position of the NGC 4696 pointing using values from the *Spitzer* SPOT software) taken for standard star calibrations in the same observing campaign to effect sky subtraction. However, for the SH data, the analogous background observations were too short compared with the NGC 4696 data and added considerable noise when subtracted. We therefore leave these as not sky subtracted. One

**Figure 2.** *Spitzer* spectrograph apertures overlaid on an $H\alpha + [N II]$ image of the central region of NGC 4696 (Crawford et al. 2005). North is up and east to the left-hand side. Small boxes show the positions of the SH spectrograph aperture while the larger boxes show the positions of the LH spectrograph aperture.

consequence of not having a concurrent sky-background observation is that the rogue pixels in the detectors are not well corrected (or corrected at all in the case of the SH data). We therefore used the `IRSCLEAN_MASK` software from the *Spitzer* contributed software site¹ to interpolate over the rogue pixels for these observations.

The data from the SH and the LH spectrographs are not rectilinear in either the spatial or spectral direction and therefore require software which has a knowledge of the detailed distortions in order to be able to extract one-dimensional spectra. We used the *Spitzer* SPICE software (version 1.3beta1 and version 1.4) for this, extracting all the spectral orders over the full aperture in both spectrographs. The final step in the SPICE software extraction is a ‘tuning’ that applies a

¹ <http://ssc.spitzer.caltech.edu/archanaly/contributed/browse.html>.

Table 2. Ratio of $H\alpha + [N II]$ fluxes in the *Spitzer* apertures measured from the original maps of Conselice et al. (2001) (NGC 1275) and Crawford et al. (2005) (NGC 4696) to those smoothed with a Gaussian kernel of FWHM of 3.10 arcsec (for the SH spectra) and a FWHM of 6.17 arcsec (for the LH spectra).

Region	Exposure id	Spectrograph	Flux ratio
NGC 1275 east	0002	SH	1.00
	0003	SH	1.06
	0004	LH	1.10
	0005	LH	1.11
	0002	SH	1.07
NGC 1275 position 2	0002	SH	1.07
	0003	SH	1.13
	0004	LH	1.04
	0005	LH	1.08
	0002	SH	1.09
NGC 1275 position 11	0002	SH	1.09
	0003	SH	1.11
	0004	LH	1.07
	0005	LH	1.01
	0002	SH	0.99
Centaurus	0002	SH	1.00
	0003	SH	1.00
	0004	LH	1.16
	0005	LH	1.06

flux calibration to the data. There are two possibilities at this stage because the size of the point spread function of the *Spitzer* telescope is of the same order as the entrance aperture size. One option applies an extended source calibration in which it is assumed that the aperture is illuminated by a uniform surface brightness source; as much flux is scattered into the aperture as is scattered out of it. The other option is to apply the point-source calibration which corrects for the fraction of flux from a well-centred point source that is lost from the aperture, as a function of wavelength.

To determine whether the point-source or extended-source calibration is more appropriate for our data, we have taken the continuum subtracted $H\alpha + [N II]$ maps and used them as proxies for the spatial distribution of the IR line emission since we do not know its spatial distribution. Assuming that the $H\alpha + [N II]$ emission is distributed spatially like the IR emission allows us to make a quantitative (but approximate) assessment of whether the emission, which appears very clearly extended on the resolution of the optical data, is actually extended at the resolution of the *Spitzer* observations. We have measured the ratio of the flux in the *Spitzer* apertures in the raw image and in the image smoothed using a Gaussian kernel of full width half-maximum (FWHM) of 3.1 or 6.17 arcsec. These widths are an approximation to the size of the *Spitzer* point spread function at 15 and 30 μm (approximately the mid-points of the SH and the LH spectra, respectively) as measured by fitting a one-dimensional Gaussian model to the azimuthal average of the central peak of a point source generated by the *Spitzer* STINYTIM point spread function modelling software. Table 2 lists these ratios for each of the exposure ids.

Examination of Table 2 shows that there is up to 16 per cent more $H\alpha + [N II]$ flux measured in the *Spitzer* apertures in the unsmoothed images compared with the smoothed images. The inverse of the *Spitzer* Slitloss Correction Function² shows that for a point source observed by *Spitzer* the factor would be 1.63 and 1.52 at 15 and 30 μm in the SH and the LH spectrographs, respectively, whereas a uniform brightness extended source would give factors

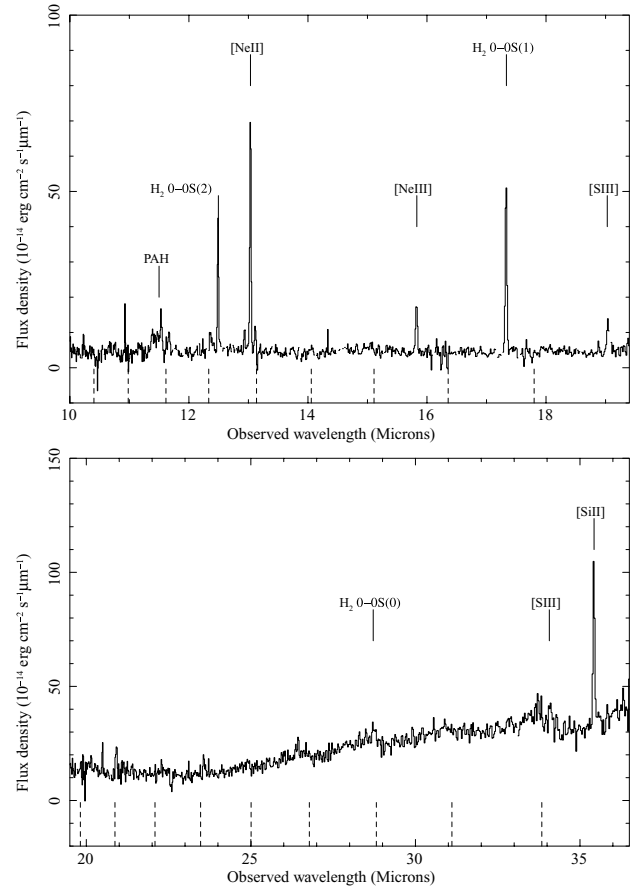


Figure 3. Upper panel: *Spitzer* SH (exposure id 0002) and lower panel: *Spitzer* LH (exposure id 0004) spectra for the NGC 1275 east pointing. The dashed vertical lines show the boundary between adjacent spectral orders.

of 1.0 for both wavelengths. This indicates that the data approximate much better to an extended source than a point source. We therefore proceed using the extended source tuning option in SPICE.

The final part of the reduction involves merging the individual spectral orders into one spectrum and converting the flux units to per unit wavelength interval. The sensitivity of the spectrograph drops significantly at the end of each order leading to an increase in the noise, but because there is an overlap in the wavelength coverage of adjacent orders (and the wavelength binning is the same at corresponding wavelengths), we are able to use the following prescription to clean the final spectrum: in the order overlap regions, we choose data from the lower order number spectrum in preference to that of the higher order number, except that we discard the six shortest wavelength bins in the highest order spectrum and the four shortest wavelength bins of all other orders. The six longest wavelength bins in the spectrum are also discarded. The spectral binning used by the SPICE extraction routine varies as a function of wavelength to preserve a constant velocity resolution of approximately 240 km s^{-1} per bin. We show examples of the final spectra in Figs 3–6, with the expected positions of some emission lines marked. The dashed vertical lines show the boundary of adjacent spectral orders.

The emission lines in the spectra were fitted individually using a Gaussian model for the line plus a straight line to account for the local continuum. The fitting was done using the QDP program³ to

² <http://ssc.spitzer.caltech.edu/irs/calib/extended.sources/index.html>.

³ <http://www.wastro.msfc.nasa.gov/qdp>.

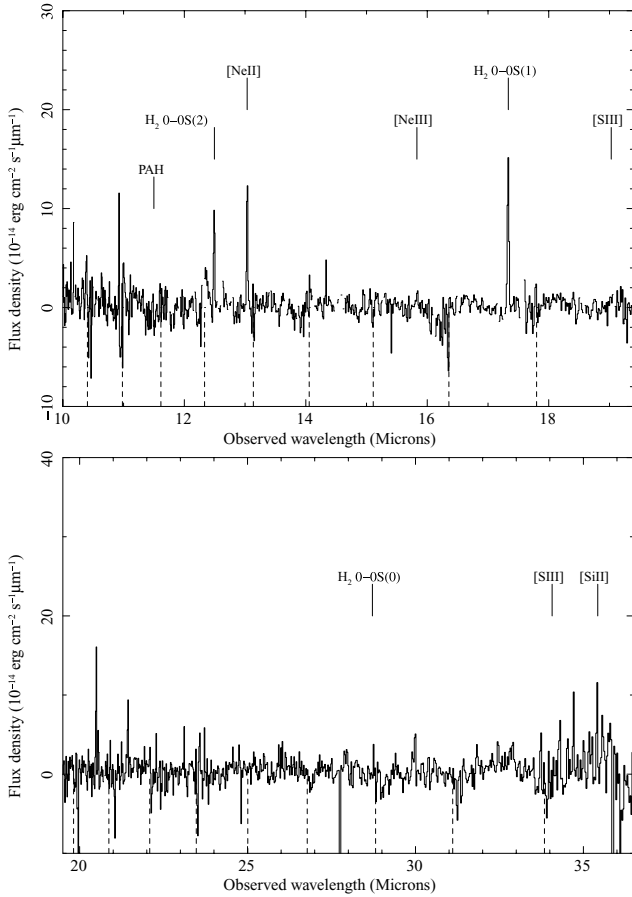


Figure 4. Upper panel: *Spitzer* SH (exposure id 0002) and lower panel: *Spitzer* LH (exposure id 0004) spectra for the NGC 1275 position 2. The dashed vertical lines show the boundary between adjacent spectral orders.

minimize the χ^2 statistic between the model and the data, subject to the propagated uncertainty in the flux at each wavelength bin. Line parameters and uncertainties are given in Tables 3–6. The uncertainties were generally calculated (for all pointings except the NGC 1275 east region) from the $\Delta\chi^2 = 1.0$ criterion (Lampton, Margon & Bowyer 1976). This corresponds to a 68 per cent confidence region or a 1σ (Gaussian equivalent) confidence region for one interesting parameter. In the cases where lines are not detected, we set a 3σ upper limit on the line flux by fixing the position and width of the line and increasing the flux until the value of χ^2 increases by nine from the value obtained with no line present. Where no uncertainty on a parameter is listed that parameter was fixed. Line widths for detected lines were left as free parameters in the fitting. However, except for the PAH 11.3 μm line the widths are not resolved beyond the instrumental resolution and are therefore not listed.

The values of the minimum χ^2 that were obtained when fitting the NGC 4696 short-wavelength spectra were significantly above the number of degrees of freedom, whereas the values of the minimum χ^2 that were obtained when fitting the NGC 1275 east spectra were significantly below the number of degrees of freedom. In both cases, this indicates that the uncertainties on each bin are wrong. In the case of the NGC 4696 short-wavelength data, there is additional power in the spectra not accounted for in the uncertainty arrays which may be due to the presence of fringes

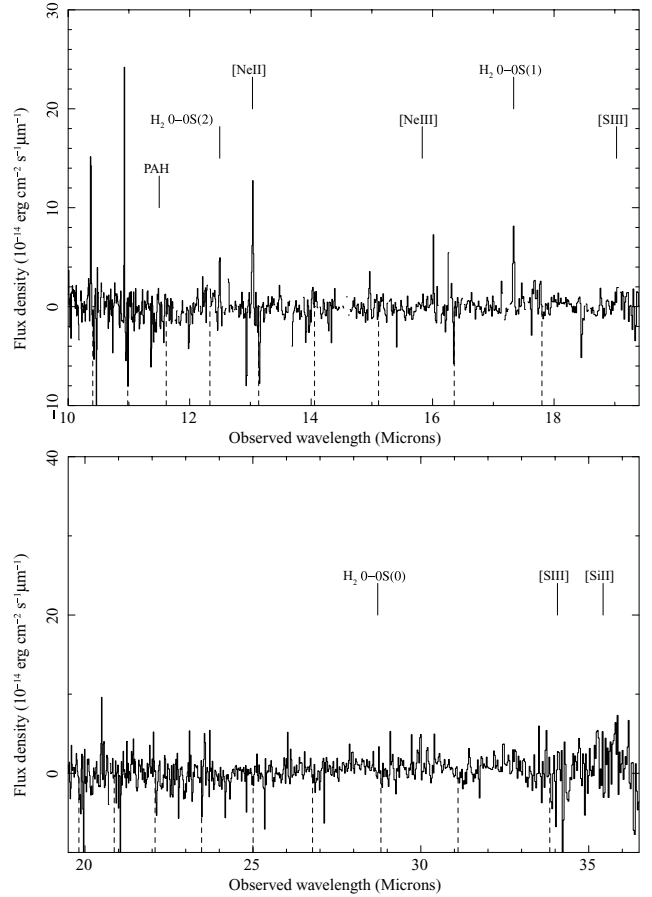


Figure 5. Upper panel: *Spitzer* SH (exposure id 0002) and lower panel: *Spitzer* LH (exposure id 0004) spectra for the NGC 1275 position 11. The dashed vertical lines show the boundary between adjacent spectral orders.

(<http://ssc.spitzer.caltech.edu/postbcd/irsfringe.html>) that have not been completely removed in the pipeline software. We tried to correct for these using the IRSFRINGE tool but were unsuccessful. In the case of the NGC 1275 east spectra, there is only one DCE and the uncertainties are propagated from the ramp fitting. This leads to uncertainties which are too big.

Since using the $\Delta\chi^2 = 1.0$ criterion under either of these conditions leads to uncertainties on the line parameters which are either too large or too small, we have adopted the ‘Ratio of Variances’ technique (Lampton et al. 1976) to rescale the critical value of delta χ^2 used to calculate the line parameter uncertainties. We note in passing that the spectral extraction method used in the SPICE software does introduce correlations between adjacent spectral bins but the *Spitzer* Science Centre advises that the degree of correlation is small because the dispersion direction in the spectral images is almost parallel with the pixel direction.

2.2 Supporting near-IR data

The *Spitzer* apertures at positions 2 and 11 in the NGC 1275 nebula cover similar sky positions to the *K*-band United Kingdom Infrared Telescope (UKIRT) CGS4 long-slit observations of the ‘horseshoe knot’ and the ‘SW1’ region of Hatch et al. (2005). Noting that the entrance apertures for the *Spitzer* spectrographs are a different shape and size to the region extracted from the CGS4 slit, we will

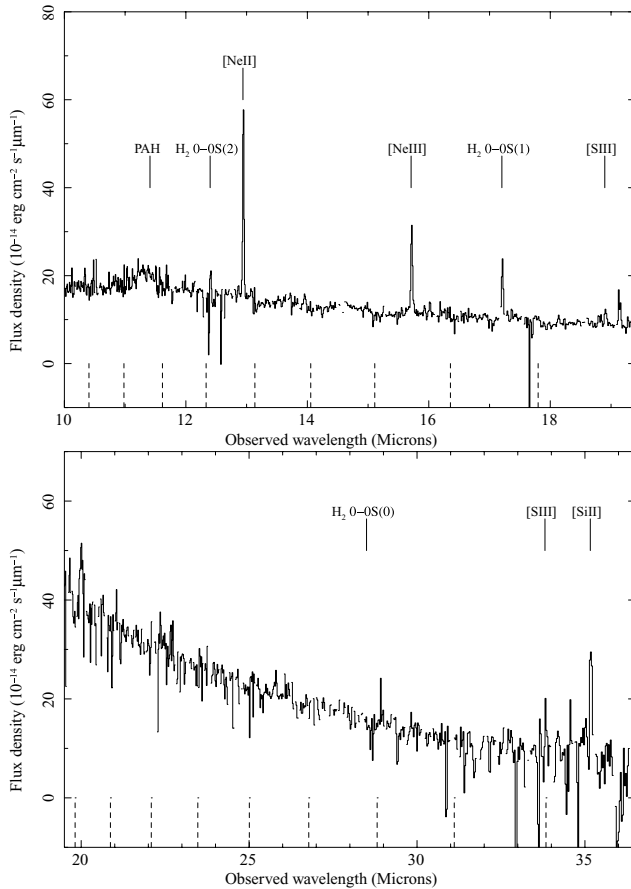


Figure 6. Upper panel: *Spitzer* SH (exposure id 0002) and lower panel: *Spitzer* LH (exposure id 0004) spectra for the NGC 4696 pointing. The dashed vertical lines show the boundary between adjacent spectral orders. Note that the SH data are not background subtracted.

later use the $P\alpha$ and H_2 ro-vibrational line fluxes of these two regions from Hatch et al. (2005) together with the *Spitzer* mid-IR H_2 rotational line fluxes of positions 2 and 11 to investigate the molecular hydrogen in these outer regions of the nebula. Full details of the observations and reduction of the K -band data from these regions are provided in Hatch et al. (2005).

The *Spitzer* aperture covering the east region does not match well to the eastern slit region of Hatch et al. (2005). Instead we have used the UKIRT 1-5 micron imager spectrometer (UIST) HK -band long-slit spectra of the bright radial filament that extends from a region 2.65 arcsec south of the galaxy nucleus eastwards to a distance of 26.8 arcsec (9.5 kpc). The observations were obtained on 2005 January 31, and the sky conditions were photometric. The long-slit was used in a 7 pixel-wide (0.84 arcsec) configuration with a spatial scale of 0.1202 arcsec pixel $^{-1}$, using the HK grating which gives a spectral coverage of 1.4 – 2.5 μm at a resolution of 700 – 1260 km s $^{-1}$. The observations were taken in non-destructive readout staring mode with an object-sky-sky-object nodding pattern. Details of the observation are provided in Table 7. Sky emission features were mostly removed by the nodding pattern, while flux calibration was achieved using a set of almost featureless F- and G-type stars of known magnitude. In each of the standards, a Br γ stellar feature at 2.166 μm was removed by linear interpolation. The data were reduced with ORAC-DR available through the UKIRT Website and Starlink packages.

A spectrum was extracted from the UIST long-slit data by summing the flux across the entire region where the more northerly *Spitzer* aperture overlaps with the UIST aperture. This results in a total long-slit aperture of 0.84×6.6 arcsec 2 . Fig. 7 shows the NGC 1275 east near-IR spectrum over the wavelength range 1.74 – 2.48 μm . The wavelength range 1.8 – 1.88 μm is a region of poor atmospheric transmission and has been masked out of the spectrum for clarity of the emission-line features. The molecular hydrogen emission lines and $P\alpha$ are clearly visible. Table 8 lists the surface brightnesses of all the emission lines. These are lower limits to the intrinsic surface brightnesses because of the unknown covering factor of the excited molecular hydrogen gas.

3 ANALYSIS

The lines detected in the *Spitzer* mid-IR spectra consist of emission from molecular hydrogen, from various atomic species of Neon, Sulphur and Silicon and from the 11.3 μm PAH feature.

3.1 Diagnostic line ratios

In order to classify the emission-line regions seen by *Spitzer*, we have plotted the lines of Neon/Sulphur/Silicon in Fig. 8, on one of the diagnostic diagrams of Dale et al. (2006). The NGC 1275 east and NGC 4696 points both lie in the Region I+II area of the diagram occupied by Seyfert and Liner nuclei. This finding is consistent with other analyses of optical emission lines in these objects which also show Liner-like spectra (e.g. Johnstone et al. 1987; Crawford et al. 1999).

3.2 [Ne III] lines

The SH spectra of the NGC 1275 east region and the NGC 4696 pointing both show strong detections of the [Ne III] λ 15.56 μm line. In the NGC 1275 east region, this is a surprising discovery since most of the very extended emission-line gas does not show emission from the optical lines of [O III] λ 4959,5007 (Hatch et al. 2006). The ionization potential of Ne $^+$ (41.07 eV) is larger than the ionization potential of O $^+$ (35.11 eV) so if lines of [Ne III] are seen, we would expect to also see lines of [O III].

There are two possible explanations for the apparent lack of the [O III] lines when the [Ne III] lines are strong, assuming that they are both formed in a photoionized nebula. The first possibility is that the [O III] and [Ne III] lines are both emitted together from a spatial region which is missed in our optical long-slit spectra but sampled in the *Spitzer* spectra due to the much larger SH aperture (4.7×11.3 arcsec) and the poorer point spread function of *Spitzer*. Alternatively, since these lines are collisionally excited and the excitation energy of the upper level in the [O III] lines (~ 29 000 K) is much greater than that for the upper level in the [Ne III] line (~ 940 K), if the electron temperature in the emitting gas is low enough, the IR [Ne III] line may be produced while the optical [O III] lines are not excited.

To determine whether the first possibility is occurring we note that the SH aperture for our NGC 1275 east observations is located very close to an H II region identified by Shields & Filippenko (1990). That H II region has much stronger [O III] emission than the surrounding nebula and therefore may contribute significant [Ne III] emission.

In order to assess whether the *Spitzer* SH apertures contain a significant amount of light from the H II region, we used the *Spitzer* STINYTIM point spread function modelling software to generate an

Table 3. Properties of emission lines in the NGC 1275 east region *Spitzer* spectra. Note that the line widths are the Gaussian sigma values.

Exposure id	Line	Wavelength (μm)	Width (σ) (μm)	Flux ($\times 10^{-14} \text{ erg cm}^{-2} \text{ s}^{-1}$)
0002	PAH 11.3	11.51 ± 0.01	0.11 ± 0.01	1.43 ± 0.16
	H ₂ 0–0 S(2) 12.28	12.4899 ± 0.0003	–	0.85 ± 0.03
	[Ne II] 12.81	13.0342 ± 0.0002	–	1.78 ± 0.03
	[Ne III] 15.56	15.8241 ± 0.0007	–	0.54 ± 0.03
	H ₂ 0–0 S(1) 17.04	17.3280 ± 0.0009	–	1.79 ± 0.09
	[S III] 18.71	19.040 ± 0.003	–	0.39 ± 0.07
0003	PAH 11.3	11.56 ± 0.03	0.14 ± 0.03	1.15 ± 0.30
	H ₂ 0–0 S(2) 12.28	12.4906 ± 0.0003	–	0.87 ± 0.03
	[Ne II] 12.81	13.0350 ± 0.0003	–	1.51 ± 0.04
	[Ne III] 15.56	15.8236 ± 0.0010	–	0.44 ± 0.03
	H ₂ 0–0 S(1) 17.04	17.3270 ± 0.0010	–	1.98 ± 0.12
	[S III] 18.71	19.040 ± 0.003	–	0.16 ± 0.04
0004	H ₂ 0–0 S(0) 28.22	28.72	–	<0.73
	[S III] 33.48	34.07	–	<1.68
	[Si II] 34.82	35.421 ± 0.001	–	4.46 ± 0.18
0005	H ₂ 0–0 S(0) 28.22	28.72	–	<0.75
	[S III] 33.48	34.07	–	<0.75
	[Si II] 34.82	35.415 ± 0.001	–	3.59 ± 0.17

Table 4. Properties of emission lines in the NGC 1275 position 2 region *Spitzer* spectra. Note that the line widths are the Gaussian sigma values.

Exposure id	Line	Wavelength (μm)	Width (σ) (μm)	Flux ($\times 10^{-14} \text{ erg cm}^{-2} \text{ s}^{-1}$)
0002	PAH 11.3	11.51	0.11	<0.11
	H ₂ 0–0 S(2) 12.28	12.4920 ± 0.0008	–	0.24 ± 0.02
	[Ne II] 12.81	13.0358 ± 0.0006	–	0.30 ± 0.02
	[Ne III] 15.56	15.8241	–	<0.19
	H ₂ 0–0 S(1) 17.04	17.3317 ± 0.0004	–	0.47 ± 0.02
	[S III] 18.71	19.040	–	<0.10
0003	PAH 11.3	11.51	0.11	<0.11
	H ₂ 0–0 S(2) 12.28	12.4925 ± 0.0010	–	0.27 ± 0.03
	[Ne II] 12.81	13.0382 ± 0.0011	–	0.21 ± 0.03
	[Ne III] 15.56	15.8241	–	<0.11
	H ₂ 0–0 S(1) 17.04	17.3334 ± 0.0006	–	0.42 ± 0.02
	[S III] 18.71	19.04	–	<0.07
0004	H ₂ 0–0 S(0) 28.22	28.72	–	<0.15
	[S III] 33.48	34.07	–	<0.27
	[Si II] 34.82	35.43	–	<0.63
0005	H ₂ 0–0 S(0) 28.22	28.72	–	<0.18
	[S III] 33.48	34.07	–	<0.36
	[Si II] 34.82	35.43	–	<0.69

image of the point spread function for the SH instrument at the observed wavelength of [Ne III] (15.8 μm). We then applied a world coordinate system to this image such that the centre of the point spread function lies at the coordinates of the H II region and the pixel scale is correct for the point spread function image. The *Spitzer* aperture region files corresponding to the two exposure ids were then applied to this image and the counts in each region were measured.

This analysis predicts that the region corresponding to exposure id 0002 (the more westerly one, nearer the H II region) should have 2.86 times the flux present in the region corresponding to exposure id 0003 if the flux comes entirely from the point source H II region. The ratio of fluxes measured in the [Ne III] lines in these two exposure ids is just 1.23. If we further assume that each exposure id has a

contribution from the extended (non-H II region) nebula proportional to the $\text{H}\alpha + [\text{N II}]$ emission listed in Table 9, then we can solve for the fractional contribution of the H II region to the [Ne III] flux in each exposure id. Under these assumptions, we find that 3 per cent of the [Ne III] flux ($1.5 \times 10^{-16} \text{ erg cm}^{-2} \text{ s}^{-1}$) in exposure id 0002 comes from the H II region while only 1 per cent of the [Ne III] flux ($5.4 \times 10^{-17} \text{ erg cm}^{-2} \text{ s}^{-1}$) in exposure id 0003 comes from the H II region. The [Ne III] flux from the extended nebula is 5.2×10^{-15} and $4.35 \times 10^{-15} \text{ erg cm}^{-2} \text{ s}^{-1}$ in exposure ids 0002 and 0003, respectively. This suggests that there is a strong extended [Ne III] emission component in the NGC 1275 east region.

We have set a 3σ upper limit on the flux in the [O III] λ 5007 line by extracting a spectrum from the Gemini data, presented by Hatch

Table 5. Properties of emission lines in the NGC 1275 position 11 region *Spitzer* spectra. Note that the line widths are the Gaussian sigma values.

Exposure id	Line	Wavelength (μm)	Width (σ) (μm)	Flux ($\times 10^{-14} \text{ erg cm}^{-2} \text{ s}^{-1}$)
0002	PAH 11.3	11.51	0.11	<0.27
	H ₂ 0–0 S(2) 12.28	12.4955 \pm 0.0013	–	0.13 \pm 0.02
	[Ne II] 12.81	13.0402 \pm 0.0008	–	0.29 \pm 0.03
	[Ne III] 15.56	15.8241	–	<0.07
	H ₂ 0–0 S(1) 17.04	17.3342 \pm 0.0008	–	0.25 \pm 0.02
0003	[S III] 18.71	19.040	–	<0.16
	PAH 11.3	11.51	0.11	<0.19
	H ₂ 0–0 S(2) 12.28	12.4958 \pm 0.0012	–	0.13 \pm 0.02
	[Ne II] 12.81	13.0411 \pm 0.0011	–	0.15 \pm 0.02
	[Ne III] 15.56	15.8241	–	<0.08
0004	H ₂ 0–0 S(1) 17.04	17.3371 \pm 0.012	–	0.21 \pm 0.02
	[S III] 18.71	19.04	–	<0.11
	H ₂ 0–0 S(0) 28.22	28.72	–	<0.07
0005	[S III] 33.48	34.07	–	<0.38
	[Si II] 34.82	35.43	–	<0.49
	H ₂ 0–0 S(0) 28.22	28.72	–	<0.14
0005	[S III] 33.48	34.07	–	<0.24
	[Si II] 34.82	35.43	–	<0.20

Table 6. Properties of emission lines in the NGC 4696 *Spitzer* spectra. Note that the line widths are the Gaussian sigma values.

Exposure id	Line	Wavelength (μm)	Width (σ) (μm)	Flux ($\times 10^{-14} \text{ erg cm}^{-2} \text{ s}^{-1}$)
0002	PAH 11.3	11.32 \pm 0.017	0.15 \pm 0.02	1.44 \pm 0.2
	H ₂ 0–0 S(2) 12.28	12.408 \pm 0.003	–	0.17 \pm 0.03
	[Ne II] 12.81	12.9469 \pm 0.0003	–	1.13 \pm 0.03
	[Ne III] 15.56	15.7184 \pm 0.0005	–	0.66 \pm 0.02
	H ₂ 0–0 S(1) 17.04	17.2122 \pm 0.0011	–	0.45 \pm 0.03
0003	[S III] 18.71	18.9110 \pm 0.004	–	0.14 \pm 0.03
	PAH 11.3	11.33 \pm 0.016	0.11 \pm 0.019	1.75 \pm 0.21
	H ₂ 0–0 S(2) 12.28	12.411 \pm 0.004	–	0.18 \pm 0.04
	[Ne II] 12.81	12.9488 \pm 0.0003	–	0.98 \pm 0.03
	[Ne III] 15.56	15.7207 \pm 0.0004	–	0.58 \pm 0.02
0004	H ₂ 0–0 S(1) 17.04	17.2142 \pm 0.0006	–	0.42 \pm 0.02
	[S III] 18.76	18.9133 \pm 0.005	–	0.13 \pm 0.04
	H ₂ 0–0 S(0) 28.22	28.497	–	<0.12
0005	[S III] 33.48	33.811	–	<0.94
	[Si II] 34.82	35.1808 \pm 0.0030	–	1.81 \pm 0.15
	H ₂ 0–0 S(0) 28.22	28.497	–	<0.10
0005	[S III] 33.48	33.811	–	<1.60
	[Si II] 34.82	35.1740 \pm 0.0021	–	3.05 \pm 0.18

et al. (2006), close to the Perseus east region (and avoiding the H II region). In order to avoid having to correct for different spatial region sizes between the optical and the IR data, we proceed by taking ratios of the [O III] and [Ne III] lines to the H α + [N II] lines:

$$\frac{F(5007)}{F(15.56)} = \frac{F(5007)}{F(\text{H}\alpha + [\text{N II}])} \bigg/ \frac{F(15.56)}{F'(\text{H}\alpha + [\text{N II}])},$$

where the ratio $F(5007)/F(\text{H}\alpha + [\text{N II}])$ is the ratio of the flux in the [O III] λ 5007 line to the flux in the sum of the H α + [N II] λ λ 6548, 6584 lines both measured from the Gemini spectrum. The ratio $F(15.56)/F'(\text{H}\alpha + [\text{N II}])$ is measured from the [Ne III] flux in the *Spitzer* spectrum and the values given in Table 9. We find a 3σ upper limit on the ratio $F(5007)/F(15.56) < 1.2$.

Gas that is photoionized by a stellar or power-law continuum generally has a temperature around 8000 K (Osterbrock & Ferland 2006). The lack of optical [O III] emission at a position where IR [Ne III] lines are seen suggests that the electron temperature is low enough to prevent optical emission from being produced. Models using the code CLOUDY (Ferland et al. 1998) show that if the abundance of O⁺⁺/Ne⁺⁺ has the solar ratio, then the ratio $F(5007)/F(15.56) \sim 10^4 T_e^{-1/2} e^{(-29000/T_e)}$. The observed limit of 1.2 in this ratio therefore corresponds to $T_e < 6300$ K.

Low temperatures in a photoionized gas are produced when the abundances are at or above solar and the gas density is low enough that most of the cooling luminosity is radiated by the fine-structure lines (Ferland et al. 1984; Shields & Kennicutt 1995). These

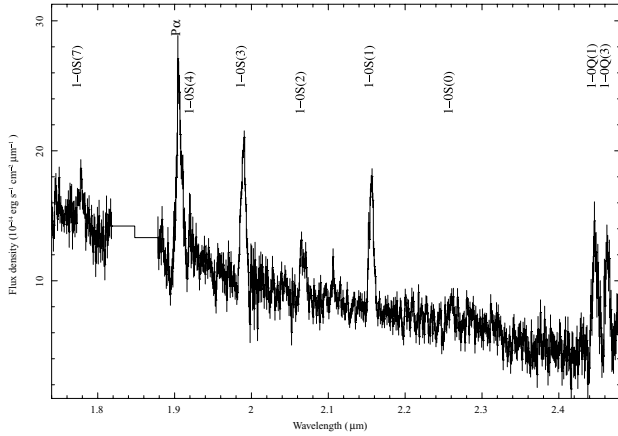


Figure 7. Near-IR spectrum of the NGC 1275 east region. The region between 1.8 and 1.88 μm has poor atmospheric transmission and has been masked out of the spectrum for clarity. Errors are from Poisson statistics.

Table 7. Details of the UIST long-slit observation of the NGC 1275 east region. The orientation of the nodding direction is described in the UIST manual.⁴ Position angle is measured east from north.

Target position (J2000)	Slit angle ($^{\circ}$)	Nod off-set (arcsec)	Exposure time (min)	Seeing (arcsec)
03 19 48.16	+70	+38, -23	144	0.4
41 30 40.1				

Table 8. Near-IR line surface brightnesses for the NGC 1275 east region together with 1σ uncertainties. The value for the 2–1 S(1) line is a 3σ upper limit.

Line	Surface brightness $\times 10^{-16} \text{ erg cm}^{-2} \text{ s}^{-1} \text{ arcsec}^{-2}$
Pa α	1.73 ± 0.08
H ₂ 1–0 S(0)	0.24 ± 0.05
H ₂ 1–0 S(1)	$1.26^{+0.08}_{-0.03}$
H ₂ 1–0 S(2)	0.55 ± 0.05
H ₂ 1–0 S(3)	1.43 ± 0.05
H ₂ 1–0 S(4)	0.23 ± 0.08
H ₂ 1–0 S(7)	$0.35^{+0.03}_{-0.04}$
H ₂ 1–0 Q(1)	1.17 ± 0.11
H ₂ 1–0 Q(3)	1.09 ± 0.11
H ₂ 2–1 S(1)	<0.12

calculations show that metallicities in the range of solar to twice solar can produce a drop in the [O III] line strength by up to 2 orders of magnitude depending on the details of the physical system.

The results from the discussion above rely on the observed optical line ratios (which have been corrected for reddening within our Galaxy) not being affected by any obscuration within the emission-line regions themselves. The Balmer decrement, calculated from the ratio of $H\alpha/H\beta$ in the Gemini spectrum, is very high (6.7) even after correcting for Galactic reddening. If this high value of the

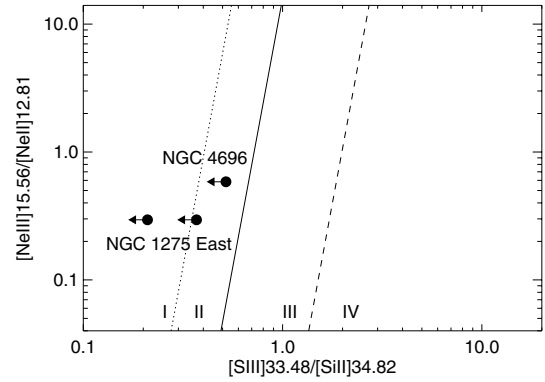


Figure 8. Neon/Sulphur/Silicon diagnostic diagram of Dale et al. (2006). Regions I+II demark the locus of Seyfert and Liner nuclei. Region III demarks the locus of H II nuclei while Region IV is the locus of Extranuclear and H II regions.

Balmer decrement is attributed to extinction in a screen in front of the emission-line region, then the implied extinction is $A_V = 2.67$. After correcting the optical lines for this amount of reddening, we obtain a limit on the ratio $F(5007)/F(15.56) < 19$ which would not set an interesting limit on the electron temperature in the nebula. We note that high values of the Balmer decrement may be produced by mechanisms other than reddening, for example, collisional excitation (Table 5, Parker 1964).

In NGC 4696, Johnstone & Fabian (1988) report $[O III]\lambda 5007/H\beta \sim 0.2$ in a 13.2×1.5 arcsec region at position angle 85° centred 5 arcsec south of, but including, the nucleus, while Lewis, Eracleous & Sambruna (2003) set an upper limit of $[O III]\lambda 5007/H\beta < 0.4$ in a region 1.8×1.0 arcsec centred on the nucleus. This indicates that the [O III] line is quite weak in this object also. We do not attempt to calculate the $F(5007)/F(15.56)$ ratio due to the much larger uncertainties because of the proximity of the *Spitzer* aperture to the galactic nucleus (Fig. 2). The inner region of the Centaurus cluster is known to have a high metallicity from X-ray observations (e.g. Sanders & Fabian 2006), although the exact value derived for the very central regions is dependent on the precise model fitted. If future observations were to be able to constrain the metallicity of the emission-line gas, that information might prove an interesting constraint on the origin of the emission-line gas.

3.3 Density diagnostic

We note that the $[S III]\lambda 18.71/[S III]\lambda 33.48$ line ratio is a density diagnostic. In the NGC 1275 east and NGC 4696 pointings, we have detections of $\lambda 18.71$ and upper limits for $\lambda 33.48$. Taking the ratio of the average of the line fluxes (or upper limits), having used the $H\alpha + [N II]$ fluxes in the *Spitzer* apertures to scale the fluxes to account for the different spatial sampling as in Section 2.1, gives $[S III]\lambda 18.71/[S III]\lambda 33.48 > 0.6$ for NGC 1275 east. CLOUDY (Ferland et al. 1998) models show that this ratio corresponds to a density of $> 100 \text{ cm}^{-3}$. No constraint is placed on the density for the NGC 4696 pointing as we are unable to scale the fluxes for the aperture effects due to saturation.

3.4 PAH features

11.3 μm PAH features are detected in the spectra of NGC 1275 east and NGC 4696. The flux is strong and comparable to that of [Ne II]. No detection is made for Perseus positions 2 and 11 which

⁴ <http://www.jach.hawaii.edu/UKIRT/instruments/uist/spectroscopy/spectroscopy.html>.

Table 9. $H\alpha$ + $[N\text{ II}]$ emission-line fluxes in *Spitzer* apertures measured from maps of Conselice et al. (2001) (NGC 1275) and Crawford et al. (2005) (NGC 4696). To account for the *Spitzer* point spread function, the maps were smoothed with a Gaussian kernel of FWHM of 3.10 arcsec for the short-wavelength aperture measurements and 6.17 arcsec for the long-wavelength aperture measurements. No measurement is available for the NGC 4696 LH apertures as these cover a region of the image in which the off-line image is saturated. The NGC 1275 values have been corrected for a reddening corresponding to $A_R = 0.4$.

Region	Exposure id	Spectrograph	Flux ($\times 10^{-13}$ erg cm $^{-2}$ s $^{-1}$)
NGC 1275 east	0002	SH	5.8
	0003	SH	4.8
	0004	LH	16
	0005	LH	15
NGC 1275 position 2	0002	SH	1.1
	0003	SH	1.0
	0004	LH	2.7
NGC 1275 position 11	0002	SH	0.83
	0003	SH	0.68
	0004	LH	1.7
NGC 4696	0005	LH	1.4
	0002	SH	1.7
	0003	SH	1.5
	0004	LH	–
	0005	LH	–

are at greater distances from the centre of the galaxy than Perseus east. The limit on position 2 is less than about one-third that of $[\text{Ne II}]$ indicating that either the abundance of PAHs or the excitation mechanism is much reduced there. Peeters, Spoon & Tielens (2004) argue that PAH features are tracers of star formation, particularly of B stars. Parts of NGC 1275 have an A-type spectrum (Minkowski 1968) which indicates some, possibly sporadic, star formation; the situation in NGC 4696 is uncertain due to the obvious dust lanes. The correlation between the presence of a PAH feature and a stellar continuum in the IRS spectrum in NGC 1275 supports an excitation mechanism involving the far UV light from moderately young stars.

In a *Spitzer* study using IRS and Multiband Imaging Photometer (MIPS) observations of seven nearby dusty elliptical galaxies including NGC 4696, Kaneda et al. (2007) find PAH emission from the centre and evidence for by dust emission which is more extensive than the starlight of the galaxy in the MIPS data.

3.5 Molecular hydrogen lines

To investigate the molecular hydrogen in more detail, we can combine the mid-IR pure-rotational emission lines with emission lines from the $1-0\text{S}(J)$ ro-vibrational states visible in the K band (Section 2.2).

3.5.1 Excitation process

Molecular hydrogen can be collisionally excited, or radiatively excited by absorption of UV photons in the Lyman–Werner bands. If the density is low enough ($< 10^4$ cm $^{-3}$) the molecule will de-excite through the ground electronic ro-vibrational states by radiative de-excitations, whereas if the density is high, the populations of the rotational and vibrational states will be redistributed by collisions before de-excitation to the ground level. The form of the observed spectrum depends on the excitation source as well as on the density and temperature of the gas. At high temperatures and

densities, the collision rate of the H_2 molecule with other molecules and atomic species increases. Collisional de-excitation therefore becomes more important than radiative de-excitations as the temperature and density increase. The total gas density at which the collisional de-excitation rate equals the radiative de-excitation rate is known as the critical density and is a slow function of temperature (Sternberg & Dalgarno 1989; Mandy & Martin 1993). When collisional excitation and de-excitation dominates, the gas exists in local thermodynamic equilibrium (LTE) and the molecular hydrogen has an ortho-to-para ratio of 3.

3.5.2 Scaling the mid-IR H_2 emission to compare with the near-IR emission

As discussed in Section 2.1, we have assumed that the mid-IR line emission is distributed spatially like the $H\alpha$ + $[N\text{ II}]$ emission. The near-IR H_2 line emission has been shown to closely follow the $P\alpha$ emission in other brightest cluster galaxies (Jaffe, Bremer & Baker 2005). Additionally, near-IR H_2 emission lines are only detected in NGC 1275 in the regions of brightest $H\alpha$ emission (Hatch et al. 2005). To examine the relationship between the atomic hydrogen emission and the near-IR molecular hydrogen emission within NGC 1275 in detail, we have analysed the whole length of the NGC 1275 east HK -band long-slit data. The long-slit data were segregated into seven regions in which $P\alpha$ was detected. Fig. 9 plots the $P\alpha$ flux and $P\alpha/1-0\text{S}(1)$ line ratio against projected distance from the galaxy nucleus for all seven regions. This figure shows that the $P\alpha/1-0\text{S}(1)$ ratio is almost constant at 1.45 across a large part of the emission-line region. We therefore assume that the $P\alpha$ emission and near-IR H_2 line emission are closely related spatially in NGC 1275. We can scale and combine the near- and mid-IR H_2 emission lines using the flux of the hydrogen recombination lines in the *Spitzer* and near-IR apertures.

To obtain Hydrogen line fluxes for the different spectra in different regions, we proceed as follows: for the *Spitzer* spectra, we used the

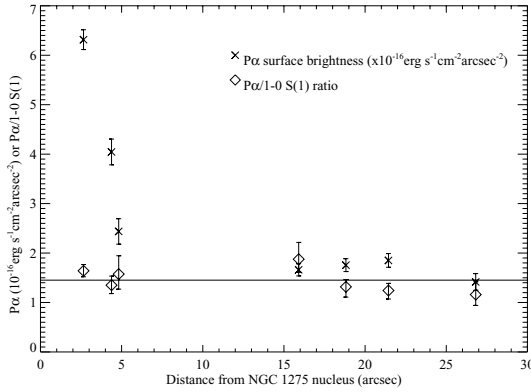


Figure 9. $P\alpha$ flux and $P\alpha/1-0 S(1)$ ratio along the UIST long-slit covering the NGC 1275 east region. The solid line shows the mean $P\alpha/1-0 S(1)$ of 1.45. Error bars are at the 1σ level. The ratio of atomic-to-molecular hydrogen line emission is fairly constant across a large range of $P\alpha$ emission.

$H\alpha + [N II]$ fluxes from the figures given in Table 9 divided by two to account for the $[N II]$ lines (Hatch et al. 2006). For the near-IR spectra, we used the $P\alpha$ flux from Table 8 for the Perseus east region, the $P\alpha$ flux given by Hatch et al. (2005) for the position 2 region and 1.45 times the flux in the $H_2 1-0 S(1)$ line (Fig. 9) for the position 11 region. This corresponds to the ‘Horseshoe knot’ in Hatch et al. (2005) which does not have a measured $P\alpha$ intensity as the line was badly affected by the poor atmospheric transmission in that part of the spectrum. To scale the $P\alpha$ flux to the $H\alpha$ flux, we assume Case B recombination theory (Osterbrock & Ferland 2006) which implies that $H\alpha/P\alpha = 8.45$. We finally scale the *Spitzer* line fluxes to match the near-IR spatial regions with:

$$F_{ss} = F_{sm} \times \frac{F_{nir}(H\alpha)}{F_s(H\alpha)},$$

where F_{ss} is the resulting scaled *Spitzer* line flux, F_{sm} is the measured *Spitzer* line flux, $F_{nir}(H\alpha)$ is the estimated $H\alpha$ flux in the near-IR aperture, $F_s(H\alpha)$ is the estimated $H\alpha$ flux in the *Spitzer* aperture.

3.5.3 Excitation temperatures, column densities and mass of warm molecular hydrogen

If collisions share the energy between the particles causing the H_2 to be in LTE, the excited states of H_2 [$N(v, J)$] will be populated in a thermalized Boltzmann distribution characterized by an excitation temperature (T_{ex}) such that:

$$\frac{N(v, J)}{g_J} = a(T_{ex}) e^{-E(v, J)/k_B T_{ex}}, \quad (1)$$

where $E(v, J)$ is the upper energy of the (v, J) transition, k_B $a(T_{ex})$ is equal to N_{Total}/Z_T , where N_{Total} is the total H_2 column density, Z_T is the H_2 partition function and g_J is the statistical weight. $N(v, J)$ is the column density of the (v, J) level, which, for optically-thin emission can be observationally determined from I [the surface brightness ($\text{erg s}^{-1} \text{cm}^{-2} \text{sr}^{-1}$)] through

$$N(v, J) = \frac{4\pi\lambda I}{A_{ul}hc}, \quad (2)$$

where λ is the rest wavelength of the line and A_{ul} is the Einstein co-efficient taken from Turner, Kirby-Docken & Dalgarno (1977). If the H_2 level populations are completely dominated by collisional excitation and de-excitation then the excitation temperature equals the kinetic temperature of the gas.

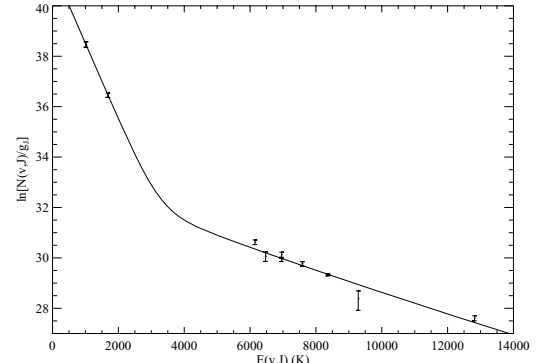


Figure 10. Population diagram of the NGC 1275 east region with 1σ error bars. The data points at $E = 1015$ and 1682 K are measured by *Spitzer* and the error bars include the uncertainty in scaling the mid-IR emission to the near-IR emission using hydrogen recombination lines.

Population diagrams of $\ln[\frac{N(v, J)}{g_J}]$ versus $E(v, J)/k_B T_{ex}$ allow investigation of whether the levels are thermalized. If the levels are thermalized, the level populations will lie in a straight line with a slope inversely proportional to the excitation temperature. If a range of gas temperatures occur along the line-of-sight, the points will lie on a smooth curve with the lower energy levels lying on a steeper slope (lower temperature) than the higher energy levels (higher temperature). This is because the higher energy levels are preferentially populated at higher temperatures.

Population diagrams for the NGC 1275 east, position 2 and position 11 regions are presented in Figs 10–12. As the population of the states lie on a smooth-curve, these diagrams clearly show that the molecular hydrogen exists in LTE at a range of temperatures. Supporting evidence that the H_2 is thermally excited comes from the ratio of the $H_2 2-1 S(1)/1-0 S(1)$ line intensity ratio. 3σ upper limits for the $2-1 S(1)$ emission lines were measured from the position 2, 11 and the NGC 1275 east regions and the limits on the $2-1 S(1)/1-0 S(1)$ ratios are given in Table 10. The measured ratio is significantly less than the pure-radiative de-excitation value of 0.53 (Mouri 1994), so the gas is predominately de-excited through collisions, perhaps with a small non-thermal component. This implies that the gas must have a density of greater than 10^4cm^{-3} .

To gain a simple picture of the structure of the molecular gas, we have measured the rotational temperature from the $0-0 S(1)$ and $0-0 S(2)$ lines and a ro-vibrational temperature from the $1-0$ lines.

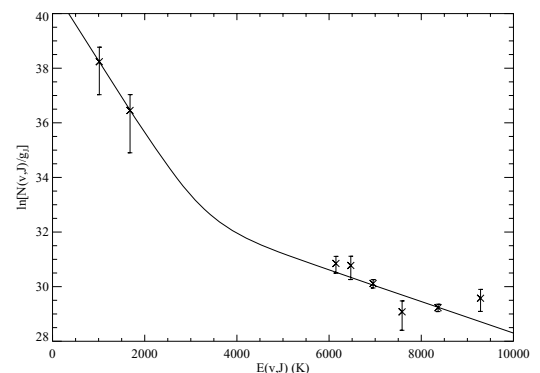


Figure 11. Population diagram of NGC 1275 position 2 with 1σ error bars. The data points at $E = 1015$ and 1682 K are measured by *Spitzer* and the error bars include the uncertainty in scaling the mid-IR emission to the near-IR emission using hydrogen recombination lines.

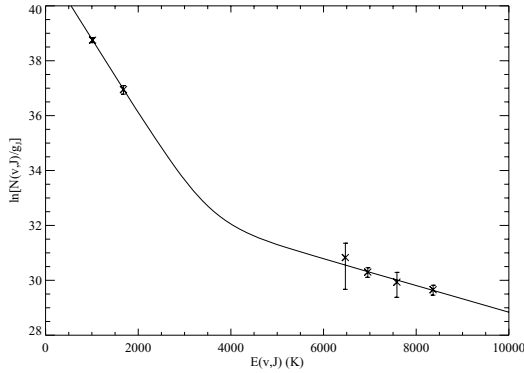


Figure 12. Population diagram of NGC 1275 position 11 with 1σ error bars. The data points at $E = 1015$ and 1682 K are measured by *Spitzer*, but the error bars do not include any uncertainty associated with scaling the mid-IR emission lines.

Table 10. The intensity ratio of H_2 $2-1 S(1)/1-0 S(1)$ lines in the three regions of NGC 1275. The $2-1 S(1)$ line fluxes are 3σ upper limits as the line is not detected in any region.

Region	$2-1 S(1)/1-0 S(1)$
NGC 1275 east	<0.097
Position 2	<0.26
Position 11	<0.44

In the NGC 1275 east *HK*-band spectrum, we measured the $1-0 S(7)$ line, and therefore we measure two ro-vibrational excitation temperatures in this region: one from levels with an upper energy of <8000 K and one from levels with an upper energy of >8000 K. These excitation temperatures are given in Table 11. The pure-rotational temperatures of the gas are $330-370$ K for all regions.

Table 11. Excitation temperatures, column densities and masses of molecular Hydrogen. The observed mass is calculated directly from the observed flux in the relevant aperture. The scaled mass is the mass scaled to the region in which the ro-vibrational lines were observed. Error bars are at the 1σ level.

	Rotational emission lines	Ro-vibrational ($2000 < E_U < 8000$ K)	Ro-vibrational ($E_U > 8000$ K)
NGC 1275 east			
T_{ex}	330 ± 20 K	$1730 \pm {}^{280}_{210}$ K	$2580 \pm {}^{160}_{145}$ K
Column density	$4.2 \times 10^{18} \text{ cm}^{-2}$	$4.4 \times 10^{15} \text{ cm}^{-2}$	$3.4 \times 10^{15} \text{ cm}^{-2}$
Observed mass of H_2	$1.5 \times 10^6 M_{\odot}$	$135 M_{\odot}$	$55 M_{\odot}$
Scaled mass of H_2	$5.0 \times 10^4 M_{\odot}$	$135 M_{\odot}$	$55 M_{\odot}$
NGC 1275 position 2			
T_{ex}	370 ± 20 K	$1730 \pm {}^{310}_{230}$ K	
Column density	$2.6 \times 10^{18} \text{ cm}^{-2}$	$1.3 \times 10^{16} \text{ cm}^{-2}$	
Observed mass of H_2	$2.9 \times 10^5 M_{\odot}$	$131 M_{\odot}$	
Scaled mass of H_2	$2.6 \times 10^4 M_{\odot}$	$131 M_{\odot}$	
NGC 1275 position 11			
T_{ex}	$370 \pm {}^{40}_{30}$ K	$2060 \pm {}^{950}_{490}$ K	
Column density	$4.5 \times 10^{18} \text{ cm}^{-2}$	$1.1 \times 10^{16} \text{ cm}^{-2}$	
Observed mass of H_2	$1.5 \times 10^5 M_{\odot}$	$53 M_{\odot}$	
Scaled mass of H_2	$2.2 \times 10^4 M_{\odot}$	$53 M_{\odot}$	
NGC 4696			
T_{ex}	310 ± 10 K		
Column density	$3.5 \times 10^{18} \text{ cm}^{-2}$		
Observed mass of H_2	$1.3 \times 10^5 M_{\odot}$		

The ro-vibrational lines reveal a layer of hotter gas at $1700-2000$ K and in NGC 1275 east there is an additional layer of even hotter gas at ~ 2600 K. Such high population temperatures are often interpreted as due to non-thermal excitation, for instance by starlight (van Dishoeck 2004) or cosmic rays (Dalgarno, Yan & Liu 1999). In the remainder of this paper, we will refer to the high v, J populations as an indication of warm H_2 , without meaning to specify what actually causes these level populations.

The total H_2 column density of the molecular hydrogen can be calculated through rearranging equation (1) and assuming that all the molecular hydrogen exists in LTE at the excitation temperature derived from the population diagrams.

$$N_{\text{Total}} = \frac{N(v, J)Z(T)}{g_J e^{-E(v, J)/k_B T_{\text{ex}}}}, \quad (3)$$

where $Z(T)$ is the partition function.

As the molecular hydrogen exists at multiple temperatures, we have assumed the gas consists of two (or three in the case of NGC 1275 east) separate populations, each consisting of a Boltzmann distribution at the excitation temperatures derived from the population diagrams. A least-squares fit was performed with the total column densities of each Boltzmann distribution as the two (or three) free parameters. Column densities at each excitation temperature for the three regions are given in Table 11.

The mass of warm molecular hydrogen within the *Spitzer* aperture can be derived from a single line luminosity and the excitation temperature. The total molecular hydrogen mass M_{Total} is derived from:

$$M_{\text{Total}} = M_{H_2} n_{\text{total}}, \quad (4)$$

where M_{H_2} is the mass of a hydrogen molecule and n_{total} is the total number of H_2 molecules. n_{total} can be derived from the luminosity from the (v, J) state through:

$$n_{\text{total}} = \frac{L(v, J)Z_{T_{\text{ex}}}}{A_{ul} h \nu g_J e^{-E(v, J)/k_B T_{\text{ex}}}}, \quad (5)$$

Table 12. Limits on the temperature and molecular hydrogen masses from the 0–0 S(0) lines. The observed mass limits are calculated directly from the upper limit to the observed flux in the relevant aperture. The scaled mass is the mass scaled to the region in which the ro-vibrational lines were observed.

Region	Temperature	Observed mass of H ₂	Scaled mass of H ₂
NGC 1275 east	> 180 K	< 2.9 × 10 ⁷ M _⊙	< 3.2 × 10 ⁵ M _⊙
NGC 1275 position 2	> 155 K	< 1.0 × 10 ⁷ M _⊙	< 3.8 × 10 ⁵ M _⊙
NGC 1275 position 11	> 150 K	< 5.6 × 10 ⁶ M _⊙	< 3.2 × 10 ⁵ M _⊙

where $L(v, J)$ is the luminosity in the (v, J) line, $Z_{T_{\text{ex}}}$ is the partition function, A_{ul} is the Einstein co-efficient and ν is the frequency of the line. The masses of the ~ 350 K material in each of the *Spitzer* apertures were calculated from the 0–0 S(1) line. The masses of the warmer gas (1700–2000 K) were measured using the 1–0 S(1) line. A check was made using the other detected lines 1–0 S(2), 1–0 S(3), 1–0 S(4) and the masses derived from these lines were within 10 per cent of the masses derived from the 1–0 S(1) line. Finally, the mass of the 2580 K material seen in the NGC 1275 east region was measured from the 1–0 S(7) line. The masses of molecular hydrogen derived from the different temperature lines are given in Table 11 as the ‘‘Observed mass of H₂’’. In the rows labelled ‘‘Scaled mass of H₂’’, we list the masses of molecular hydrogen at each temperature scaled to the region in which the ro-vibrational lines were measured; the *Spitzer* masses were scaled down by the ratio of H α fluxes in the relative apertures, as described in Section 3.5.2. The majority of the molecular gas exits at lower temperatures with less than 0.5 per cent of the total mass being at the higher temperatures.

Without the measurement of the 0–0 S(0) line, it is not possible to derive the temperature and mass of the coldest component of the warm H₂ gas. Therefore, we use the 3σ upper limits on the 0–0 S(0) flux to obtain lower limits on the temperature and upper limits on the mass of the coldest component of the warm molecular hydrogen. These limits are displayed for the NGC 1275 pointings in Table 12. We cannot carry out the scaling for the NGC 4696 pointing as the region of the H α + [N II] map covered by the LH aperture is affected by saturation. The minimum allowed temperature of the coolest component is 150–180 K, and approximately 10 times more mass may exist at this cool temperature than in the warmer molecular hydrogen.

3.5.4 Correlation with optical emission lines

In Fig. 13, we plot the molecular hydrogen 0–0 S(1) flux against the H α + [N II] flux for all the NGC 1275 and NGC 4696 pointings. The flux in the *Spitzer* 0–0 S(1) molecular hydrogen line seems to correlate well with the flux in the optical H α + [N II] lines. The fit is a straight line constrained to go through the origin and shows that the flux in the 0–0 S(1) line is 0.03 times the flux in the H α + [N II] complex.

3.5.5 Pressure balance between the molecular, atomic and X-ray emitting gas

There is a serious problem implied by the apparent thermal distribution of the levels in the molecular hydrogen. This is that the currently used collisional rates for the ro-vibrational states require that the density exceeds 10^{4-5} cm⁻³ (Sternberg & Dalgarno 1989; Mandy & Martin 1993). If the temperature is few times 1000 K then

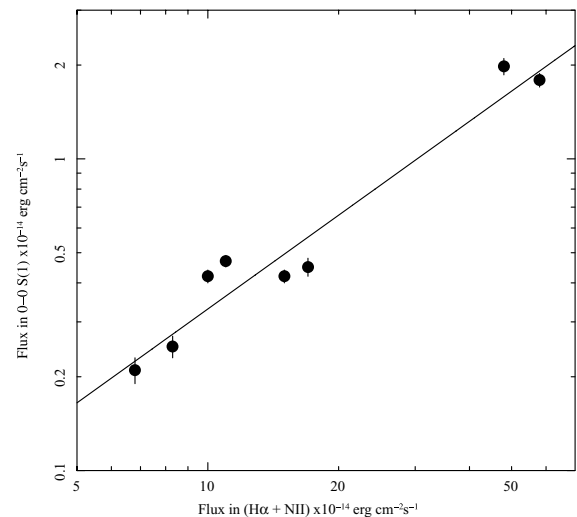


Figure 13. Flux in 0–0 S(1) line plotted against the flux in the H α + [N II] complex for all the NGC 1275 and 4696 pointings. The solid line is a straight-line fit in linear coordinate space, constrained to pass through the origin. It has a slope of 0.03.

the pressure is 10^{7-8} cm⁻³ K. This exceeds the ambient pressure, as determined from the X-ray measurements of the hot gas (Sanders, Fabian & Dunn 2005), by an order of magnitude or more. This does not appear to be a stable situation for such thin, apparently long-lived, filaments.

Recent studies have brought the H₂ collision database into question. The Orion Bar is the closest and best studied H⁺/H⁰/H₂ interface (O’Dell 2001). Allers et al. (2005) found that H₂ rotational lines implied level populations that were close to a thermal distribution. They noted that the density within the Bar is too low to thermalize the levels involved if the current H₂ collision rates are correct. They suggest that current H–H₂ vibrational de-excitation rates should be increased by nearly two orders of magnitude (their table 6). If this were the case then H₂ level populations could reach a thermal distribution at the low densities implied by the pressure of the hot gas. Our data are further evidence that the de-excitation rates may require a large correction.

3.6 Heating mechanisms

A detailed discussion of the heating mechanism of the emission-line gas in central galaxies in cooling core clusters is beyond the scope of this paper. In the nuclear regions, the situation can be complex with several different mechanisms at work. These include photoionization from an active nucleus (for NGC 1275) (e.g. Wilman, Edge & Johnstone 2005), photoionization by stars (e.g. Johnstone

et al. 1987; Allen 1995; Wilman et al. 2002) and possibly shocks (e.g. Jaffe et al. 2001; Wilman et al. 2002).

We expect that the off-nuclear regions which we have targeted in the observations presented in this paper will be more representative of the general emission-line nebula and also simpler to understand. We note that the apparently thermalized nature of the molecular hydrogen lines argues against their formation in a classical photodissociation region and that the relation between the $H\alpha + [N II]$ flux and the flux in the molecular hydrogen lines presented in Fig. 13 could suggest that shocks are important. However, it is not clear that there would be enough cloud–cloud collisions in these regions to drive this mechanism. Shocks also need to be constrained to a fairly narrow range of velocity, fast enough to produce the optical emission lines, but not so fast that dust is destroyed. Jaffe et al. (2001) have previously discussed the requirement for the fine tuning of shock velocities in trying to explain the ro-vibrational molecular lines in a sample of cooling core central cluster galaxies.

In a future paper, we will explore these difficulties in more detail and examine the possibility of excitation via cosmic rays which leak out of the radio lobes and ghost bubbles (e.g. Birzan et al. 2004; Dunn, Fabian & Sanders 2005).

4 CONCLUSION

Using high-resolution mid-IR spectra from the *Spitzer Space Telescope*, we have detected off-nuclear emission lines in NGC 1275 and NGC 4696. The lines arise from pure-rotational transitions of the Hydrogen molecule, atomic fine-structure transitions from Ne^{++} , S^{++} and Si^{+} and the $11.3 \mu m$ PAH feature.

The relative intensities of the molecular hydrogen lines are consistent with collisional excitation and probe a new region of temperature space in the filaments at 300–400 K. Pressure equilibrium with the surrounding intracluster medium requires a substantial revision to H_2 collision rates, as noted by Allers et al. (2005). The outer filaments around NGC 1275 therefore have molecular gas at 50 K (CO, from P. Salomé et al., in preparation), 300–400 K (H_2 , this paper) and 2000–3000 K (H_2 , Hatch et al. 2005), atomic gas at several 1000 K ($H\alpha$, e.g. Conselice et al. 2001) and $\sim 10^7$ K (Fabian et al. 2003b), embedded in the hot intracluster gas at about 5×10^7 K. Detection of O^{5+} from more central regions with For Ultra-violet Spectroscopic Explorer (Bregman et al. 2006) suggests that gas at $\sim 3 \times 10^5$ K is also likely to be present.

The discovery of the $[Ne III]$ lines is unexpected based on the weakness of the optical $[O III]$ lines, and suggests that the electron temperature in the filamentary medium where these lines are formed may be very low, possibly due to enhanced metallicity. The metal abundance of the central intracluster medium in cooling cluster cores is enhanced by Type Ia supernovae, and possibly Type II supernovae (see Sanders & Fabian 2006, and references therein), so the filaments are enriched if they originate from cooling of that gas.

Collectively the mid-IR emission lines radiate about one-quarter of the flux in $H\alpha$, so they play a relatively minor role in the energy flow in the filaments. However, the total molecular hydrogen emission, including the near IR ro-vibrational lines is comparable to the emission from $H\alpha$. ($H\alpha$ is about one-tenth of the total line emission: the major emitter is expected to be $Ly\alpha$.) Nevertheless, they reveal more about the low-temperature core to the filaments which is dominated in mass by H_2 . The total mass in H_2 for NGC 1275, obtained from the CO emission using a standard Galactic conversion ratio, is $\sim 4 \times 10^{10} M_{\odot}$ (Salomé et al. 2006), most of it near the centre of the galaxy. The mass in H_2 at 300 K is about $6 \times 10^7 M_{\odot}$, assuming that the masses found for the outer filaments in this paper scale linearly

with $H\alpha$ emission, and using the total $H\alpha$ flux of Conselice et al. (2001). The total mass of $H\alpha$ emitting gas is smaller at about $3 \times 10^7 M_{\odot}$ and the mass of surrounding soft X-ray emitting gas, with temperature $\sim 7 \times 10^6$ K, is about $10^9 M_{\odot}$ (Fabian et al. 2006).

Further observations are required to test whether all filaments have similar composition and properties, but they do appear to be predominantly molecular.

ACKNOWLEDGMENTS

ACF and CSC acknowledge support by the Royal Society. RMJ and NAH acknowledge support by the Particle Physics and Astronomy Research Council. GJF thanks the NSF (AST 0607028), NASA (NNG05GD81G), STScI (HST-AR-10653) and the *Spitzer* Science Centre (20343) for support. We thank an anonymous referee for comments which improved the paper.

REFERENCES

- Allen S. W., 1995, MNRAS, 276, 947
 Allers K. N., Jaffe D. T., Lacy J. H., Draine B. T., Richter M. J., 2005, ApJ, 630, 368
 Bauer F. E., Fabian A. C., Sanders J. S., Allen S. W., Johnstone R. M., 2005, MNRAS, 359, 1481
 Birzan L., Rafferty D. A., McNamara B. R., Wise M. W., Nulsen P. E. J., 2004, ApJ, 607, 800
 Böhringer H., Voges W., Fabian A. C., Edge A. C., Neumann D. M., 1993, MNRAS, 264, L25
 Bregman J. N., Fabian A. C., Miller E. D., Irwin J. A., 2006, ApJ, 642, 746
 Conselice C. J., Gallagher J. S. III, Wyse R. F. G., 2001, AJ, 122, 2281
 Cowie L. L., Hu E. M., Jenkins E. B., York D. G., 1983, ApJ, 272, 29
 Crawford C. S., Fabian A. C., 1992, MNRAS, 259, 265
 Crawford C. S., Allen S. W., Ebeling H., Edge A. C., Fabian A. C., 1999, MNRAS, 306, 857
 Crawford C. S., Hatch N. A., Fabian A. C., Sanders J. S., 2005, MNRAS, 363, 216
 Churazov E., Brüggem M., Kaiser C. R., Böhringer H., Forman W., 2001, ApJ, 554, 261
 Churazov E., Sunyaev R., Forman W., Böhringer H., 2002, MNRAS, 332, 729
 Dale D. A. et al., 2006, ApJ, 646, 161
 Dalgarno A., Yan M., Liu W., 1999, ApJS, 125, 237
 Donahue M., Mack J., Voit G. M., Sparks W., Elston R., Maloney P. R., 2000, ApJ, 545, 670
 Dunn R. J. H., Fabian A. C., Sanders J. S., 2005, MNRAS, 366, 758
 Edge A. C., 2001, MNRAS, 328, 762
 Edge A. C., Wilman R. J., Johnstone R. M., Crawford C. S., Fabian A. C., Allen S. W., 2002, MNRAS, 337, 49
 Egami E., Rieke G. H., Fadda D., Hines D. C., 2006, ApJ, 652, 21L
 Fabian A. C., 1994, ARA&A, 32, 277
 Fabian A. C., Hu E. M., Cowie L. L., Grindlay J., 1981, ApJ, 248, 47
 Fabian A. C., Nulsen P. E. J., Atherton P. D., Taylor K., 1982, MNRAS, 201, 17
 Fabian A. C. et al., 2000, MNRAS, 318, L65
 Fabian A. C., Sanders J. S., Ettori S., Taylor G. B., Allen S. W., Crawford C. S., Iwasawa K., Johnstone R. M., 2001, MNRAS, 321, 33
 Fabian A. C., Celotti A., Blundell K. M., Kassim N. E., Perley R. A., 2002a, MNRAS, 331, 369
 Fabian A. C., Allen S. W., Crawford C. S., Johnstone R. M., Morris R. G., Sanders J. S., Schmidt R. W., 2002b, MNRAS, 332, L50
 Fabian A. C., Sanders J. S., Allen S. W., Crawford C. S., Iwasawa K., Johnstone R. M., Schmidt R. W., Taylor G. B., 2003a, MNRAS, 344, 43
 Fabian A. C., Sanders J. S., Crawford C. S., Conselice C. J., Gallagher J. S. III, Wyse R. F. G., 2003b, MNRAS, 344, 48

- Fabian A. C., Sanders J. S., Taylor G. B., Allen S. W., Crawford C. S., Johnstone R. M., Iwasawa K., 2006, *MNRAS*, 366, 417
- Ferland G. J., Williams R. E., Lambert D. L., Shields G. A., Slovak M., Gondhalekar P. M., Truran J. W., 1984, *ApJ*, 281, 194
- Ferland G. J., Korista K. T., Verner D. A., Ferguson J. W., Kingdon J. B., Verner E. M., 1998, *PASP*, 110, 761
- Hatch N. A., Crawford C. S., Fabian A. C., Johnstone R. M., 2005, *MNRAS*, 358, 765
- Hatch N. A., Crawford C. S., Johnstone R. M., Fabian A. C., 2006, *MNRAS*, 367, 433
- Heckman T. M., Baum S. A., van Breugel W. J. M., McCarthy P., 1989, *ApJ*, 338, 48
- Hu E. M., Cowie L. L., Wang Z., 1985, *ApJS*, 338, 48
- Jaffe W., Bremer M. N., 1997, *MNRAS*, 284, L1
- Jaffe W., Bremer M. N., van der Werf P. P., 2001, *MNRAS*, 324, 443
- Jaffe W., Bremer M. N., Baker K., 2005, *MNRAS*, 360, 748
- Johnstone R. M., Fabian A. C., 1988, *MNRAS*, 233, 581
- Johnstone R. M., Fabian A. C., Nulsen P. E. J., 1987, *MNRAS*, 224, 75
- Kaneda H., Onaka T., Sakon I., 2005, *ApJ*, 632, 83L
- Kaneda H., Onaka T., Kitayama T., Okada Y., Sakon I., 2007, *PASJ*, 59, 107
- Krabbe A., Sams B. J. III, Genzel R., Thatte N., Prada F., 2000, *A&A*, 354, 439
- Lampton M., Margon B., Bowyer S., 1976, *ApJ*, 208, 177
- Lewis K. T., Eracleous M., Sambruna R. M., 2003, *ApJ*, 593, 155
- Lynds R., 1970, *ApJ*, 159, L151
- McNamara B., O'Connell R., Sarazin C. L., 1996, *AJ*, 112, 91
- Mandy M. E., Martin P. G., 1993, *ApJS*, 86, 199
- Mouri H., 1994, *ApJ*, 427, 777
- Minkowski R., 1957, in van de Hulst H. C., ed., *Proc. IAU Symp. 4, Radio Astronomy*. Cambridge Univ. Press, Cambridge, p. 107
- Minkowski R., 1968, *AJ*, 73, 842
- O'Dell C. R., 2001, *ARA&A*, 39, 99
- Osterbrock D., Ferland G. J., 2006, in Osterbrock D. E., Ferland G. J., eds, *Astrophysics of Gaseous Nebulae and Active Galactic Nuclei*, 2nd. edn. University Science Books, Sausalito, CA
- Parker R. A. R., 1964, *ApJ*, 139, 208
- Pedlar A., Ghataure H. S., Davies R. D., Harrison B. A., Perley R., Crane P. C., Unger S. W., 1990, *MNRAS*, 246, 477
- Peres C. B., Fabian A. C., Edge A. C., Allen S. W., Johnstone R. M., White D. A., 1998, *MNRAS*, 298, 416
- Peeters E., Spoon H. W. W., Tielens A. G. G. M., 2004, *ApJ*, 613, 986
- Peterson J. A. et al., 2001, *A&A*, 365, L104
- Sabra B. M., Shields J. C., Filippenko A. V., 2000, *ApJ*, 545, 157
- Salomé P., Combes F., 2003, *A&A*, 412, 657
- Salomé P. et al, 2006, *A&A*, 454, 437
- Sanders J. S., Fabian A. C., 2006, *MNRAS*, 371, 1483
- Sanders J. S., Fabian A. C., Dunn R. J. H., 2005, *MNRAS*, 360, 133
- Shields J. C., Filippenko A. V., 1990, *ApJS*, 353, 7
- Shields J. C., Kennicutt R. C., 1995, *ApJ*, 454, 807
- Shobbrook R. R., 1966, *MNRAS*, 131, 351
- Sparks W. B., Macchetto F., Golombek D., 1989, *ApJ*, 345, 153
- Sternberg A., Dalgarno A., 1989, *ApJ*, 338, 197
- Turner J., Kirby-Docken K., Dalgarno A., 1977, *ApJS*, 35, 281
- van Dishoeck E. F., 2004, *ARA&A*, 42, 119
- Weedman D. W. et al., 2005, *ApJ*, 633, 706
- Wilman R. J., Edge A. C., Johnstone R. M., Fabian A. C., Allen S. W., Crawford C. S., 2002, *MNRAS*, 337, 63
- Wilman R. J., Edge A. C., Johnstone R. M., 2005, *MNRAS*, 359, 755

This paper has been typeset from a $\text{\TeX}/\text{\LaTeX}$ file prepared by the author.